ACS APPLIED ENERGY MATERIALS

www.acsaem.org Article

Influence of the Side Chain Structure on the Electronic Structure and Self-Organization Properties of Low Band Gap Polymers

Sven Bölke, David Batchelor, Andreas Früh, Benedikt Lassalle-Kaiser, Tina Keller, Florian Trilling, Michael Forster, Ullrich Scherf, Thomas Chassé, and Heiko Peisert*

Cite This: *ACS Appl. Energy Mater.* 2022, 5, 15290−15301 Read Online

ACCESS | Metrics & More | Article Recommendations | Supporting Information

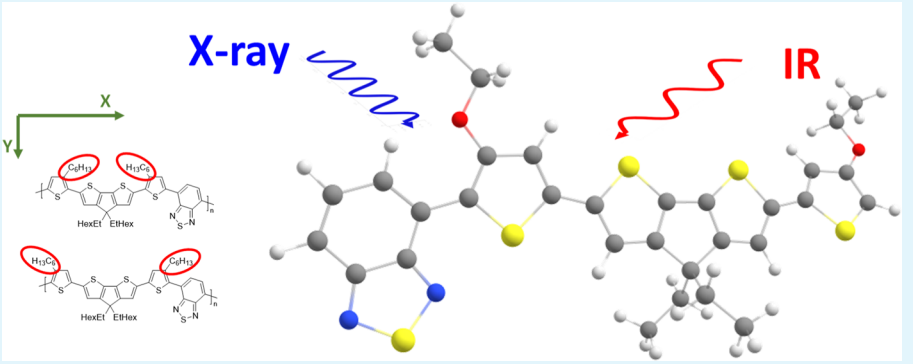

ABSTRACT: The properties of low band gap polymers in devices such as solar cells are strongly influenced by their morphology and ability of self-organization in thin films and interface properties. We study the influence of alkyl and alkoxy side chain position for four conjugated, alternating oligothiophene-benzothiadiazole copolymers on the molecular orientation in thin films and electronic interface properties using photoemission, X-ray absorption spectroscopy (XAS) at the sulfur K edge, and polarization modulation-infrared reflection−absorption spectroscopy (PMIRRAS). The interface charge transfer (ICT) model is used to explain interface properties of the polymers on substrates with different work functions. We find that the position of the side chains has a significant influence on the orientation and thus on self-organization properties of the polymers in thin films, whereas the electronic structure is less affected. The preferred molecular orientation is further affected by annealing, leading to a higher degree of ordering. Results from complementary methods with different surface sensitivities (XAS in total electron yield and fluorescence mode and PMIRRAS) are discussed.

KEYWORDS: *organic solar cells, low band gap polymers, UPS, NEXAFS, electronic structure, orientation*

1. INTRODUCTION

Properties such as flexibility, coloration, and semi-transparency make polymers ideal candidates for novel optoelectronic devices. As an example, a promising application field of polymer-based organic solar cells (OSCs) is building integrated photovoltaics with visible-light transparency.[1−3] For donor−acceptor-based bulk heterojunction (BHJ) organic photovoltaic cells, low band gap (LBG) polymers are established as a material for the donor component. They exhibit an increased absorption in the visible and near infrared regions of the solar spectrum compared to polymers with larger gaps.[4] Typically, LBG polymers consist of electron-deficient and electron-rich moieties, utilizing the intramolecular push−pull effect. Based on a similar chemical approach, non-fullerene acceptor materials were recently developed, enabling a further increase in the effective absorption of light and an optimized donor−acceptor interaction.[3,5,6] As a result, power conversion efficiencies of organic solar cells are now comparable with other types of solar cells.[3,7,8] A fine-tuning of both the chemical structures of photoactive materials and electronic properties is pre-requisite for applications in organic photovoltaic devices.[8,9]

In this context, the self-organization in polymer thin films is an important issue, affecting, among others, the length scale of phase separation, the composition of both phases, lateral distribution of the components through the interface, and the mobility of positive and negative charge carriers. Besides the processing conditions, pre- and post-processing treatments of

Received: September 8, 2022
Accepted: November 28, 2022
Published: December 13, 2022

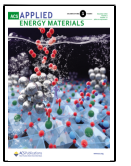

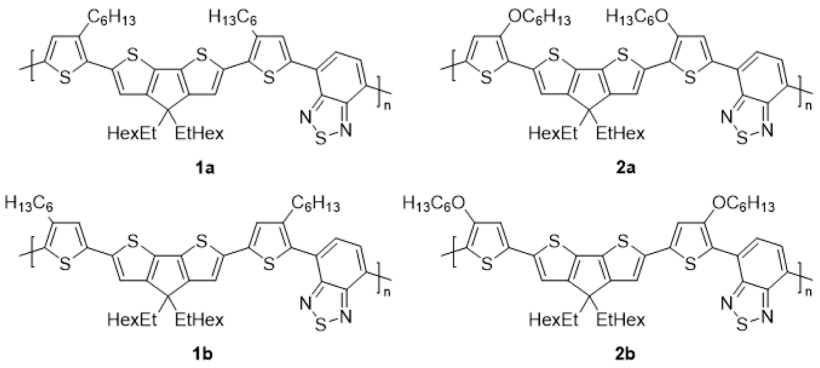

Figure 1. Studied copolymers. The side chain at the thienylene spacers (alkyl and alkoxy) is varied for **1a**/**2a** and **1b**/**2b** as well as their position (**1a**/**1b** and **2a**/**2b**).

the substrates and organic layers, the chemical structure determines the arrangement of the polymer chains.

The aim of this study is the investigation of relations between the chemical structure of LBG polymers and the ordering in thin films. We suppose that self-organization properties determined for pristine polymer films are also important for blends, since driving forces in both cases are intermolecular interactions. This was already observed for the polymer-fullerene blend, even if the degree of ordering decreases after blending.[10] In such cases, the exact chemical structure of the blend materials may affect the molecular orientation and ordering.

Several spectroscopic techniques enable the investigation of the ordering and orientation of polymers; very often, X-ray diffraction is applied (e.g., refs 11 and 12). Alternatively, X-ray absorption spectroscopy (XAS) (or near-edge X-ray absorption fine structure, NEXAFS) can be utilized to probe molecular orientation of the polymer backbone in thin films, which is, in particular, useful for blend systems with small domain sizes.[10,13−17] Most XAS studies in the literature have been carried out in the soft X-ray region at the low atomic number K edges, for example, carbon and nitrogen[18,19] in the total electron yield (TEY) mode with an information depth of about 10 nm.[20] Another method for the determination of the molecular orientation of polymers is polarization modulation-infrared reflection−absorption spectroscopy (PMIRRAS).[21−25]

To ensure maximal bulk sensitivity, we performed XAS measurements at the S K edge in the fluorescence yield (FY) mode and compared them to surface-sensitive measurements in the TEY mode. These results are compared to PMIRRAS, another bulk-sensitive method. Since side chains may affect significantly the film-forming properties in thin films of LBG polymers,[26,27] we vary the substitution pattern in conjugated, alternating oligothiophene-benzothiadiazole copolymers. In addition, the influence of the substitution on electronic properties is studied by X-ray photoelectron spectroscopy (XPS), ultraviolet photoelectron spectroscopy (UPS), and ultraviolet−visible spectroscopy (UV/vis).

2. EXPERIMENTAL SECTION

2.1. Materials and Sample Preparation. The four studied dithienylcyclopentadithiophene (dithienyl-CPDT)-benzothiadiazole (BT) copolymers are shown in Figure 1. The synthesis was adopted from previously established protocols,[28−31] described in detail in the Supporting Information. The substitution pattern at the thienylene spacers (alkyl and alkoxy) was varied. For ease, the polymers are abbreviated as **1a**, **1b**, **2a**, and **2b** in the following (the number refers to the spacer type, and the letter refers to the position). The choice of polymers was motivated by the crucial role of hexyl-thiophene moieties in the ability of self-organization in thin films.[14] On the other hand, the exchange of alkyl side chains by alkoxy chains may improve the photostability of polymers.[32] The polymers have similar molecular weights (14, 10, 15, and 10 kg/mol for polymers **1a**, **2a**, **1b**, and **2b**, respectively).

Polymer thin films were prepared by doctor-blade casting in a nitrogen atmosphere from 0.2 and 0.5% (w/w) solutions in chloroform, resulting in film thicknesses in the range of 5 nm (XPS and UPS) and 50 nm (XAS and PMIRRAS). For XAS and PMIRRAS, either gold-covered silicon wafers or indium tin oxide (ITO, Hoya Corporation, sheet resistance R = 10 Ω/□) were used as a substrate. Prior to deposition, the substrates were cleaned using chloroform and iso-propanol, followed by a UV/ozone treatment for 15 min. Gold substrates for XPS/UPS measurements were treated with UV/ozone for 1 h. Polyethylenimine (PEI) on ITO was doctor-blade-casted in a nitrogen atmosphere from 0.1% (w/w) solution in isobutanol at 80 °C and subsequently annealed to 110 °C for 10 min.

2.2. Methods. XPS and UPS measurements were performed using a multichamber ultrahigh vacuum (UHV) system with a base pressure of 5 × 10^{-10} mbar. The spectrometer is equipped with a helium discharge lamp (Leybold-Heraeus UVS10/35), a conventional Mg X-ray tube (Omicron DAR 400), and an Omicron hemispherical analyzer (EA 125). UPS spectra have been measured using He I radiation (21.22 eV). The energy scale was calibrated with respect to the binding energies of Au $4f_{7/2}$ (84.0 eV) and Cu $2p_{3/2}$ (932.6 eV). For the estimation of the composition, sensitivity factors from Yeh and Lindau were used.[33] For ultrathin films, the film thickness was estimated by the comparison of intensities of the substrate and overlayer compared core level spectra. The mean free path was estimated according to Seah and Dench.[34] In the case of thicker films, the thicknesses were estimated from the linear dependence of concentration of the polymer solution for doctor blade casting, checked by the thickness obtained from the extinction in UV/vis spectra.

XAS spectra at the sulfur K edge were measured at the LUCIA beamline[35] of synchrotron SOLEIL in Saint-Aubin, France. The polarization degree of the p-polarized synchrotron radiation was >0.95. The setup enables the variation of the incidence angle between 15 and 90° with respect to the sample surface. Spectra were measured in a vacuum chamber (10^{-2} mbar) in the FY and TEY mode simultaneously. The beam energy was monochromatized with a Si(111) double-crystal monochromator, and the beam size was about 2 × 4 mm. The energy of sulfur K edge spectra was calibrated to reproduce the sodium thiosulfate pre-edge peak maximum at 2470.8 eV. Differences of energy positions of former studies (refs 10,14, and 17) are ascribed to a different calibration procedure (reference $ZnSO_4$ at 2482.4 eV). All XAS spectra were divided by the incident photon flux and normalized to the same step height.

The peak fit analysis of XPS and XAS spectra was performed using UNIFIT.[36] XPS spectra were described by a Voigt profile peak shape (convolution of Gaussian and Lorentzian peaks) and a Shirley model

https://doi.org/10.1021/acsaem.2c02919
ACS Appl. Energy Mater. 2022, 5, 15290−15301

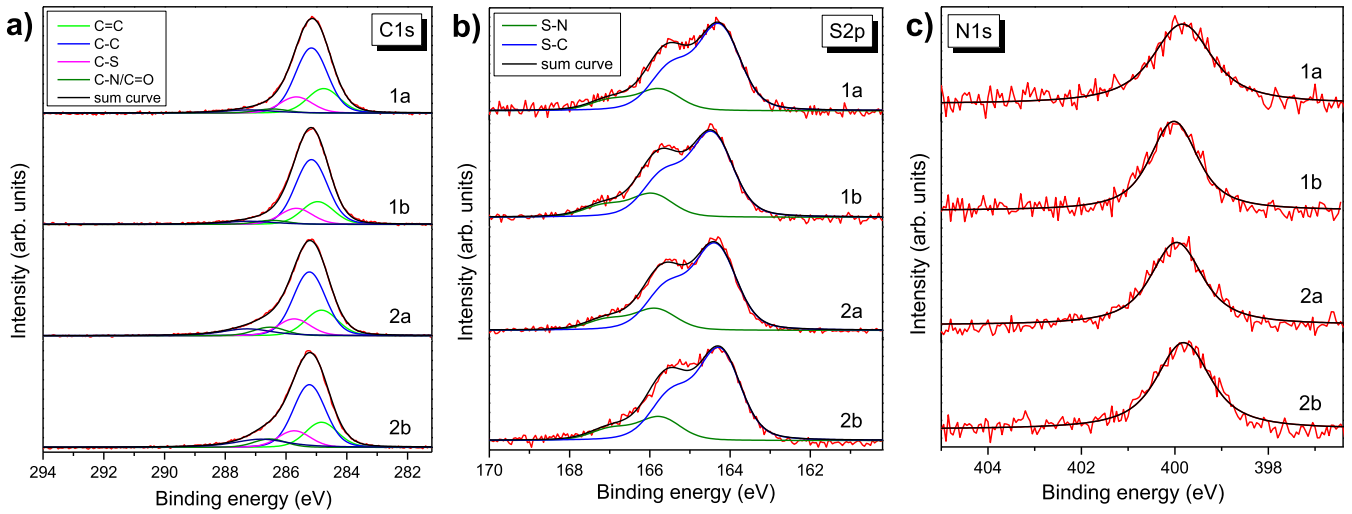

Figure 2. XPS core level spectra of thin films on gold for the four studied polymers. (a) C 1s, (b) S 2p, and (c) N 1s.

background. XAS spectra were fitted by Gaussian peaks, and the position of the step background function was calculated based on S 1s binding energies and the work function of the sample. Simulations of XAS spectra were carried out by applying time-dependent density functional theory as implemented in the ORCA program package.[37] The hybrid functional B3LYP with basis set def2-TZVP was chosen. Only excitations from localized S 1s orbitals were allowed. The geometry optimization was carried out as described below for IR spectra. In order to reproduce the experiment, the absolute energies were shifted by about 2%.

PMIRRAS was performed using a Vertex 70v spectrometer (Bruker) with the PMA50 module. Random orientation reference measurements were made using pressed KBr pellets and measured in the transmission mode. The DFT calculations were carried out for trimers and shortened side chains, using Gaussian 16[38] at the B3LYP/6-31G* level of theory. It is known that the frequencies calculated by DFT generally overestimate fundamental frequencies, for example, due to incomplete treatment of electron correlation, neglect of mechanical anharmonicity, and approaches of basis sets.[39−41] For the chosen basis set, we use a scaling factor of 0.97, in excellent agreement with the literature (e.g., refs 39−43).

3. RESULTS AND DISCUSSION

3.1. Characterization and Electronic Structure. As a first step, the composition of the four polymers in thin films was checked with XPS. In Figure 2, C 1s, S 2p, and N 1s core level spectra are shown for thin films of the four polymers on a gold substrate. Due to the presence of different, chemically inequivalent carbon species, the corresponding C 1s spectra appear comparably broad. The carbon spectra can be fitted with essentially three components: an aromatic carbon (C═C) at a binding energy of 284.8 eV, alkyl carbon (C−C, 285.2 eV), and carbon bonded to sulfur (C−S, 285.7 eV). In addition, at higher binding energies, components assigned to C−N and C−O were found, described by a single component in C 1s core level spectra. The binding energies are in good agreement with the literature.[44,45] The appearance of possible shake-up satellites was neglected in this fitting model.

From the number of chemically inequivalent carbon atoms, we expect different intensity ratios for carbon components of the C 1s spectra C−C/C═C/C−S/C−N(O) of 1/0.41/0.28/0.07 (polymers **1a** and **1b**) and 1/0.44/0.30/0.15 (polymers **2a** and **2b**). The intensities are in good agreement with the stoichiometric composition (Table 1), indicating the absence of carbon impurities.

Table 1. Relative Intensities of Carbon and Sulfur Compounds in XPS Core Level Spectra, Shown in Figure 2[a]

polymer	1a	1b	2a	2b
C−C	1	1	1	1
C═C	0.38	0.35	0.40	0.40
C−S	0.26	0.25	0.26	0.26
C−N/C−O	0.06	0.06	0.13	0.13
S 2p(T)/S 2p (BT)	3.9:1	3.7:1	3.9:1	3.9:1

[a]The number of peaks and their relative position were fixed. The values are in good agreement with the stoichiometric composition.

As for related polymers,[45] the two different sulfur species in S 2p core level spectra arising from thiophene and benzothiadiazole moieties can be well distinguished (Figure 2b). They were described by two doublets with a spin−orbit splitting of 1.20 eV. The binding energies of the S $2p_{3/2}$ component is 164.3−164.4 and 165.8−165.9 eV for thiophene (T) and benzothiadiazole (BT), respectively. The intensity ratio of both doublets is in good agreement with the stoichiometry (4:1), as summarized in Table 1. Also, the appearance of a single nitrogen species is observed for the two chemically equivalent nitrogen atoms (Figure 2c), and the overall chemical composition (Table S1, Supporting Information) indicates a successful preparation of thin films of the pristine polymers.

Electronic properties of organic semiconductors may depend crucially on slight changes in the chemical structure. An example is the introduction of fluorine atoms, resulting in a drastic increase in the ionization potential (position of the highest occupied molecular orbital (HOMO) with respect to the vacuum level).[46] However, also the optical gap and electronic interface properties can be tuned by chemical modifications.

Therefore, we investigated the influence of the side chains on the electronic structure of the four studied polymers and their interfaces using UPS together with UV/vis. For the evaluation of interface properties, we chose two substrates with significantly different work functions Φ_{sub}: PEI (Φ_{sub} = 3.3 eV) and gold (Au, Φ_{sub} = 5.2 eV). The ionization potential (IP), the optical band gap (E_g^{opt}), and Φ_{org} of the polymer films on the two substrates and the work function difference $\Delta = \Phi_{org} - \Phi_{sub}$ are summarized in Table 2. The IP was calculated by the

https://doi.org/10.1021/acsaem.2c02919
ACS Appl. Energy Mater. 2022, 5, 15290−15301

Table 2. Summary of Electronic Parameters of Studied Polymer Films Prepared at Room Temperature without Subsequent Annealing on PEI and Gold as Obtained from UPS and UV/Vis[a]

	IP			Φorg/Δ	
polymer	PEI	Au	E_g^{opt}	PEI	Au
1a	5.1	5.2	1.66	3.8/+0.5	4.6/−0.6
1b	5.1	5.3	1.94	3.7/+0.4	4.6/−0.6
2a	4.8	4.8	1.43	3.8/+0.5	4.6/−0.6
2b	4.6	4.8	1.57	3.8/+0.5	4.5/−0.7

[a]Spectra are shown in Figures S1 and S2 (Supporting Information). All values are given in eV.

sum of the work function of the polymer Φ_{org} and the onset of the HOMO position in UPS valence band spectra. A Tauc plot[47] was used to determine the optical band gap from UV/vis spectra (Figure S2, Supporting Information).

Although, for some films of highly oriented small molecules, an orientation-dependent IP was observed,[48,49] in most cases, this parameter can be regarded as a material property. We cannot completely rule out that a different (substrate-dependent) morphology of the ultrathin films may affect the ionization energy to some extent. However, the dependence of the IP on the substrate (Table 2) is small, considering an error bar of ±0.1 eV. Noticeably, the IP for the polymers with alkyl groups (**1a** and **1b**) is about 0.4 eV higher compared to polymers with alkoxy groups (**2a**, **2b**), whereas the position of the side chains has minor influence on IP. Also, the optical gap is larger for polymers with alkyl groups: Comparing **1a**/**2a** and **1b**/**2b**, it increases by 0.23 and 0.37 eV, respectively. A possible reason might be that the electron-withdrawing alkoxy group increases the electron-deficient character of the thiophene moiety, reducing both the optical gap and the ionization potential. The dependence of the optical gap on the position of the side chain (cf. **1a**/**1b** and **2a**/**2b**) might also be affected by the detailed arrangement of the polymers in the thin film. The UV/vis spectra of polymers **2a**/**2b** in Figure S2 (Supporting Information) exhibit distinct shoulders at the low energy side (higher wavelength), which might be ascribed to the high degree of aggregation.

The work function Φ_{org} of the four polymer films on PEI and Au distinctly deviate from the work function of the pristine substrates, indicating that a simple vacuum level alignment regime at these interfaces cannot be assumed and an interface dipole is formed. Surprisingly, almost independent of variations of the electronic structure (IP and E_g^{opt}), the work function upon deposition of the polymer films increases by 0.4−0.5 eV on PEI and decreases by 0.6−0.7 eV on Au. Corresponding energy level diagrams are shown in the Supporting Information (Figure S3).

A common model for the interpretation of weakly interacting interfaces formed by organic semiconductors on different substrates is the integer charge transfer (ICT) model.[50−54] Within this model, a pinning due to an integer charge transfer across the formed interface is expected if $\Phi_{sub} > ICT^+$ or $\Phi_{sub} < ICT^-$. The positive and negative integer charge transfer levels ICT^+ and ICT^- are associated with geometrically fully relaxed positive and negative polaron levels, often located 0.4−0.7 eV above the HOMO and below the LUMO (lowest unoccupied molecular orbital), respectively.[52] On the other hand, if $ICT^- < \Phi_{sub} < ICT^+$, the absence of a charge

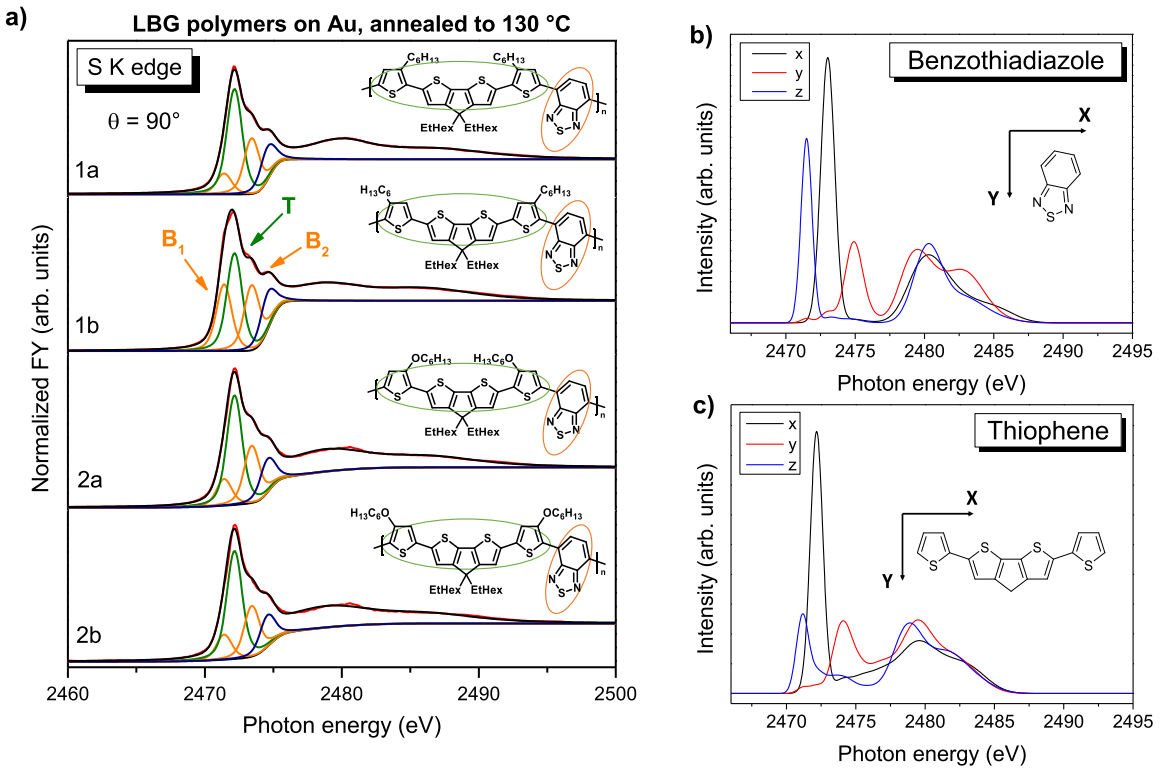

Figure 3. (a) Examples for S1s excitation spectra of LBG polymers on Au at angle Θ = 90° between the sample surface and direction of the p-polarized synchrotron light. The different sulfur moieties are shown as peak fit components, for thiophene (T) green and for benzothiadiazole (B) orange. (b) Calculated XAS spectra of cartesian vector components *x* (black), *y* (red), and *z* (blue) for benzothiadiazole and (c) for thiophene moieties.

https://doi.org/10.1021/acsaem.2c02919
ACS Appl. Energy Mater. 2022, 5, 15290−15301

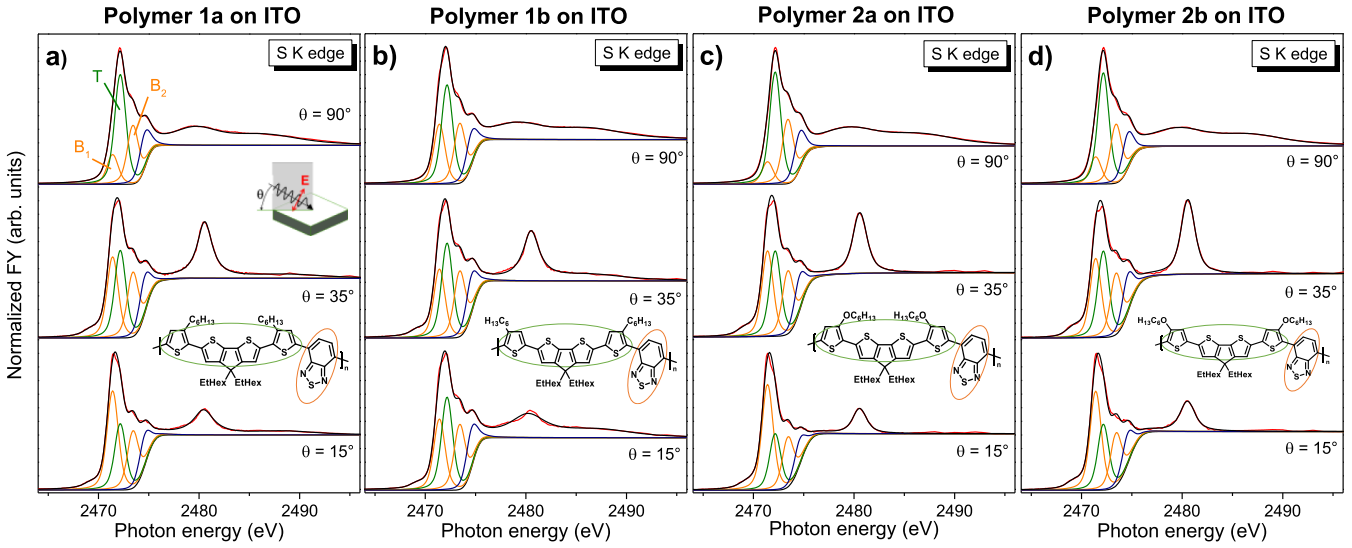

Figure 4. (a–d) S K edge XAS spectra for the four studied polymers on ITO at angles Θ = 15°, Θ = 35°, and Θ = 90° between the sample surface and direction of the (p-polarized) synchrotron light. The measurement geometry is shown as an inset. The colored ellipses in the molecule structure illustrate the origin of feature T (thiophene related, green) and feature B_1 and B_2 (benzothiadiazole related, orange).

transfer and thus a vacuum level alignment regime is expected since Φ_{sub} is settled in the band gap between polaron levels of the organic semiconductor.

We note that the mechanisms for the energy level alignment depend strongly on the strength of the interaction at the interface. In addition, the interpretation of ICT levels is a topic of debate. As an example, for molecules deposited on clean metal surfaces prepared in ultrahigh vacuum, the introduction of a dielectric spacer layer may change a chemisorption-driven fractional charge transfer to an electrostatically driven integer charge transfer mechanism.[55,56] On the other hand, in most cases, studies on particular interfaces are not suited to validate the applicability of different models for the interface energetics at the huge variety of organic–substate interfaces. Here, we focus on the comparison of the energy level alignment of four polymers with different substitution patterns, and for a deeper discussion of the nature of the integer or fractional charge transfer levels, we refer to the literature (e.g., refs 55–60).

The appearance of large dipoles Δ at all studied interfaces (Table 2) indicates a pinning at the ICT levels. For polymer thin films on the low work function substrate PEI, a pinning to ICT^- is expected, whereas on the gold substrate, a pinning to the ICT^+ level occurs. However, if a pinning regime is established in all cases, the Φ_{org} values in Table 2 imply that ICT^+ and ICT^- are located at about 3.8 eV and 4.6 eV, respectively, almost independent of the polymer structure and other electronic properties (IP and E_g^{opt}). On the other hand, ICT^- is found in a broader range of 0.2–0.6 eV above the HOMO (cf. IP − Φ_{org}(Au) in Table 2). We note that a strong variation of ICT^- with respect to IP was also reported for poly(3-hexylthiophene) as a function of annealing.[53] Thus, the results imply that the position of ICT levels, important for the energetics in devices, cannot be predicted straightforwardly from other electronic parameters. Moreover, one might speculate that the side chains do not affect the ICT levels significantly, as long as the aggregation in thin films changes dramatically.

Further information about the (unoccupied) electronic structure can be gained by XAS. Figure 3a shows S K edge absorption spectra from all four polymer thin films, annealed at 130 °C, on a gold substrate at normal incidence (Θ = 90°) and measured in the FY mode. For related polymers,[14] the spectra can be well described by a set of single peaks obtained from application of a peak fit routine, where features B_1 and B_2 (orange peaks) are assigned to transitions predominantly localized at the benzothiadiazole species (2471.4 and 2473.5 eV) and T (green peak) is assigned to thiophene species (2472.1 eV). The assignment of spectral features is confirmed by time-dependent DFT calculations (using ORCA[37]) shown in Figure 3b,c. In the upper panel, we show calculated sulfur K-edge spectra from the benzothiadiazole (BT) unit, and in the lower panel, we show calculated sulfur K-edge spectra from the thiophene (T) unit, each separated into their cartesian vector components *x* (black, in-plane parallel to the backbone), *y* (red, in-plane perpendicular to the backbone), and *z* (blue, out-of-plane). In the lower photon energy range (<2475 eV), two intense peaks are visible for BT, whereas the spectrum of T is dominated by a single peak. B and T peaks appear at different photon energies, allowing an assignment of T to thiophene and B_1 to BT moieties, as shown in Figure 3a. An energy separation of 0.7 eV is in excellent agreement with the experiment. The calculations reveal that the lowest lying feature contains, more exactly, out-of-plane (*z*-) polarized transitions of both moieties. The relative intensity of the out-of-plane transition for thiophenes is expected to be weak, in agreement to our calculations in Figure 3c. Furthermore, the calculations suggest that the intensity at the position of the B_2 component in Figure 3a is determined, to a large extent, by BT (*x*-polarized). However, the energy separation with respect to B1 and T (1.6 and 0.9 eV) deviates by 0.5 eV from the applied four component fitting model in Figure 3a, most likely due to the considerable overlap of the various contributions of BT and T moieties. Therefore, we use B1 and T features for the evaluation of polarization-dependent intensities. The fourth component in Figure 3a (blue curve) cannot be unambiguously attributed to a particular moiety on the basis of our calculations.

As might be expected from the chemical composition, all sulfur K edge XAS spectra can be described by the same model, as shown in Figure 3a, and side chains and a possible

https://doi.org/10.1021/acsaem.2c02919
ACS Appl. Energy Mater. 2022, 5, 15290–15301

different aggregation have a negligible influence on the local electronic structure at the sulfur atoms. Closer inspection of Figure 3 shows that the intensities of the B and T moieties depend on the polymer, in particular, intensities of polymer **1b** differ from those of the other three polymers. The reason for this could be a difference in the molecular orientation, which will be discussed in more detail in the following.

3.2. Molecular Orientation in Thin Films. The vector components of calculated S K XAS spectra in Figure 3b,c exhibit a strong dichroism of the observed intensities with the direction of the electric field vector of incoming light. In other words, if the XANES spectra of polymer films show strong differences depending on the angle of incoming light, then there should be a particular preferred orientation in the films.

For thiophenes and benzothiadiazoles, S1s → π^* and S1s → σ^* transitions are close in energy,[14,61−64] and thus, a prediction of the polarization of a transition is not straightforward. The DFT calculations in Figure 3b,c reveal that for the four investigated polymers, features around T are mainly polarized in-plane, parallel to the polymer backbone, whereas B_1 is mainly determined by the out-of-plane transitions. In the energy range of B_2, in-plane transitions, perpendicular to the backbone, are predicted. The behavior is similar to related polymers.[13]

Angle-dependent XAS spectra for all four polymers as prepared on ITO are shown in Figure 4 together with the peak fits. The fits yield energetic values B_1 = 2471.4 eV, T = 2472.2 eV, and B_2 = 2473.4 eV. The assignment of the main features at these photon energies was already discussed (cf. Figure 3). The "bump" at higher photon energies (about 2480 eV) is not related to the polymer and ascribed to sulfur in the glass substrate on which ITO was deposited (corresponding XAS measurements are shown in Supporting Information, Figure S4, and scanning electron microscopy and energy-dispersive X-ray (EDX) measurements are shown in Supporting Information, Figure S5).

The S K edge XAS spectra of the polymer films prepared on ITO, at room temperature (Figure 4), exhibit a distinct angular dependence of all components, except for the spectra of polymer **1b**. It seems that, in particular, the position of the alkyl side chains can have a strong influence on the orientation of the polymers; possibly, the aggregation of the polymer backbones is hindered for this substitution pattern. This is supported by the corresponding UV/vis spectra (Figure S2, Supporting Information). A possible aggregation band at the low energy side is hardly visible for the film of polymer **1b**; the spectrum is only slightly broadened compared to the spectrum measured in solution. In contrast, the significant broadening of thin film spectra of polymers with alkoxy side chains (**2a** and **2b**) indicates a higher degree of aggregation.

The XAS spectra for polymers **1a**, **2a**, and **2b**, shown in Figure 4, exhibit a similar angular dependence: The intensity maximum of T is found at normal incidence (90°), whereas the maximal intensity of B_1 is observed at grazing incidence (15°). Since T is polarized in the *x*-direction (along the polymer backbone) and B1 is out-of-plane (cf. Figure 3b,c), this behavior indicates a preferred "face-on" orientation of the polymer backbones parallel to the substrate surface. Polymer **1b** might be either disordered in the film or oriented with larger tilt angles of the orbital planes (close to the magic angle). In the latter case, however, larger tilt angles of both the backbone (*x*) and the plane of the backbone with respect to the sample surface have to be present, since we do not observe a clear angular dependence for both T and B_1.

A closer inspection of the data in Figure 4 reveals distinct differences of the dichroism. In Table 3, we summarize relative intensities of B1 and T components at normal and grazing incidence ($I(90°)/I(15°)$). Intensities were taken from peak fits of spectra shown in Figure 4. A figure with a zoom into the region of interest is shown in Supporting Information, Figure S6. The dichroism for polymer **2a** is the strongest but similar to polymers **1a** and **2b**. In contrast, for polymer **1b**, the dichroism is almost negligible, and intensity variations are less than 20% (cf. also Figure 5).

Table 3. Dichroism: Relative Peak Fit Intensities of B_1 and T Components at Normal Incidence (Θ = 90°) with Respect to Grazing Incidence (Θ = 15°) for all Four Polymers as Deposited at Room Temperature (Spectra Shown in Figure 4) and after Post-deposition Annealing to 130 °C (Spectra Shown in Figure S7, Supporting Information)

polymer		1a	1b	2a	2b
room temperature	B_1	0.36	0.88	0.25	0.34
	T	2.17	1.19	2.56	2.33
annealed (130 °C)	B_1	0.18	0.38	0.15	0.25
	T	3.51	1.50	3.07	2.43

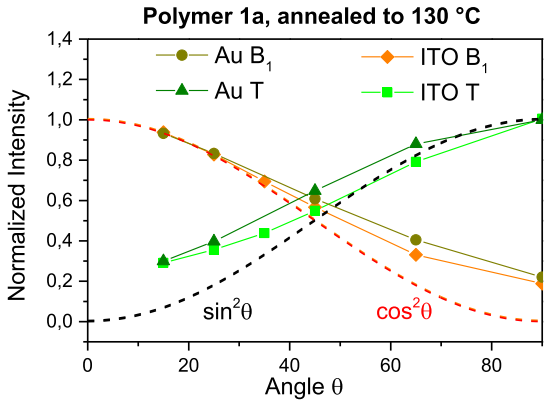

Figure 5. Comparison of the angular dependence of the intensity of T and B_1 components of polymer **1a** on ITO and gold, both annealed to 130 °C. The dashed lines are shown to guide the eyes regarding expected intensity trends in the case of "face-on" oriented polymer chains.

For many polymers, a post-deposition annealing may affect the morphology, improving long-range ordering and thus optoelectronic properties of the films.[65−72] However, the molecular orientation is not always affected by this treatment.[70] For the four studied polymers, the intensity ratio $I(90°)/I(15°)$ of B1 and T components after post-deposition annealing to 130 °C is summarized in Table 3 (bottom rows). The intensities were taken from peak fits of polarization-dependent XAS spectra, shown in Figure S7 (Supporting Information). For all four polymers, polarization-dependent intensity variations increase significantly upon annealing, that is, values in Table 3 are lower for B1 and higher for T compared to room temperature. The largest dichroism after post-deposition annealing is observed for polymers **1a** and **2a**, indicating a more pronounced "face-on" orientation compared to polymer films deposited at room temperature without post-

https://doi.org/10.1021/acsaem.2c02919
ACS Appl. Energy Mater. 2022, 5, 15290−15301

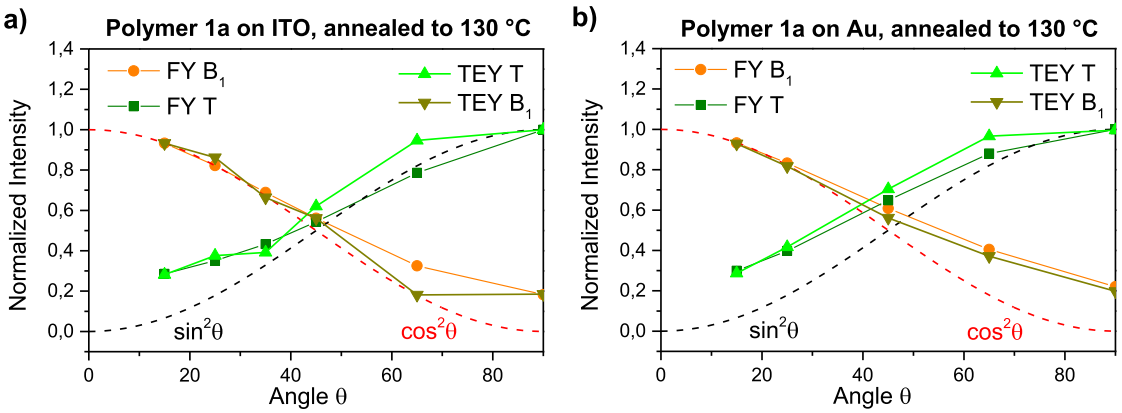

Figure 6. Comparison of the angular dependence of the intensity of T and B_1 components of polymer **1a** on ITO (a) and gold (**b**), measured in FY and TEY modes. After deposition, both films were annealed to 130 °C. The similar curves indicate an almost homogeneous orientation of the polymer chains.

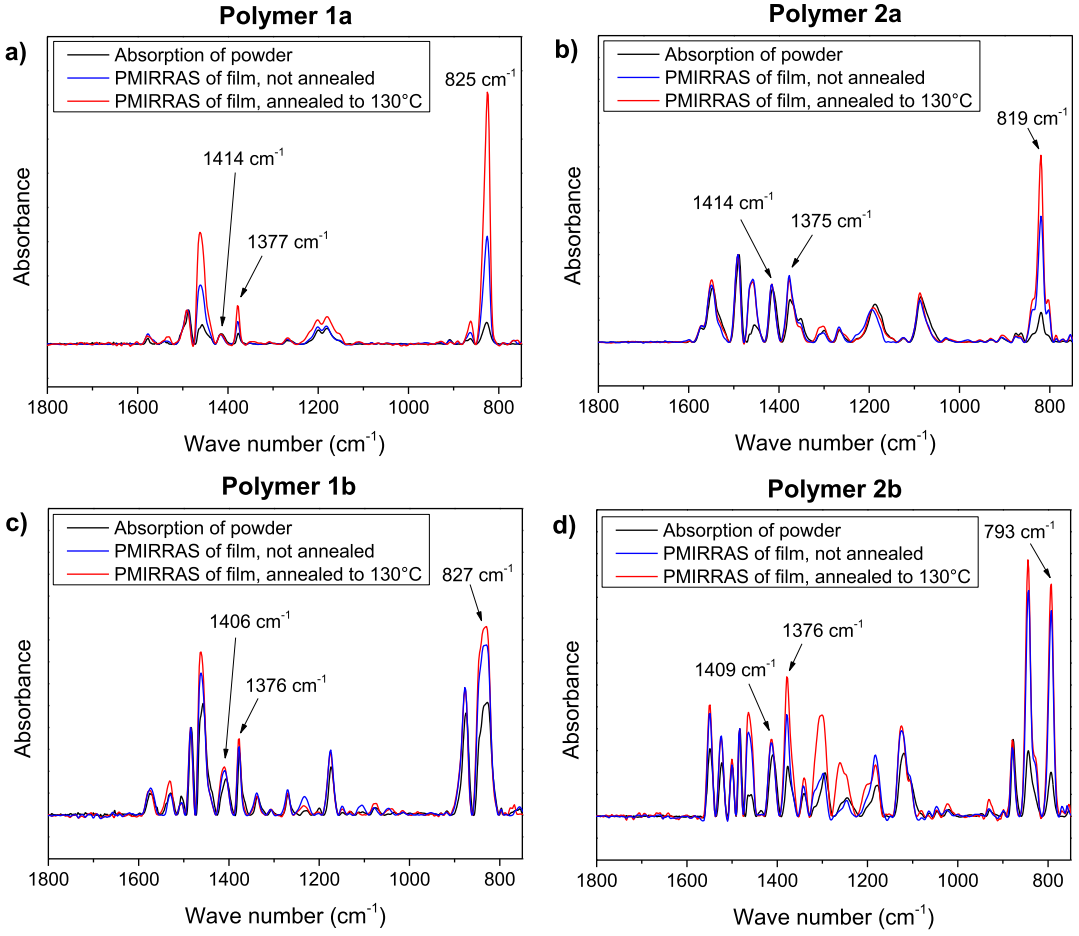

Figure 7. (a–d) PMIRRAS spectra of 50 nm-thick polymer films on gold before (blue) and after annealing (red) compared to IR spectra from polymers in KBr (black). All spectra were normalized to the maximal intensity of the band at about 1485 cm^{-1}. Clearly visible, weakest intensity variations were observed for polymer **1b** (e.g., band at 827 cm^{-1}).

annealing. After annealing, also polymer **1b** is the preferred "face-on" orientation on the substrate surface, even if this trend is less distinctive in comparison to the other polymers. These examples show that depending on the chemical structure, a post-deposition annealing might be crucial to achieve the desired morphology and ordering. For applications such as photovoltaic cells where a high amount of similar oriented molecules is crucial for the efficiency, post-deposition annealing is advantageous for all four polymers and indispensable for polymer **1b**.

3.3. Influence of the Substrate on the Molecular Orientation. The influence of the substrate was studied using polymer **1a**, a polymer which exhibits both a high dichroism at room temperature and after post-deposition annealing. Films of a similar thickness were prepared on gold and ITO substrates and subsequently annealed to 130 °C. Polarization-

https://doi.org/10.1021/acsaem.2c02919
ACS Appl. Energy Mater. 2022, 5, 15290−15301

dependent S K edge XAS spectra (Figure S7, Supporting Information) were measured at six different angles, ranging from normal incidence (Θ = 90°) to grazing incidence (Θ = 15°) (cf. inset of Figure 4). For a face-on oriented molecule and 100% linear polarization of the p-polarized synchrotron radiation, the angle-dependent intensity can be described by a simple $\cos^2\theta$ function for out-of-plane (*z*-polarized) and a $\sin^2\theta$ function for in-plane (*x* or *y* polarized) transitions.[73,74] Assuming further pure polarization of the components (T: in-plane and B_1: out-of-plane, cf. Figure 3), their normalized intensities can be compared to $\sin^2\theta$ and $\cos^2\theta$ curves, as shown in Figure 5. Data were normalized to $\sin^2(15°)$ and $\cos^2(90°)$ for B_1 and T, respectively.

The data points in Figure 5 follow fairly well the ideal $\sin^2\theta$ and $\cos^2\theta$ curves (dashed), indicating a high degree of orientation and ordering on both substrates. The results show that for the example of polymer **1a**, there is only very little influence of gold or ITO substrates on the orientation of the polymer in thin films. This is crucial for the next part of this work, where we compare two different methods, XAS and PMIRRAS. For PMIRRAS, we need a highly reflective metal substrate, and because there is no substrate dependence, we can compare our XAS data not only on gold but also on ITO substrates with our PMIRRAS measurements on gold.

3.4. Depth Dependence of the Molecular Orientation. In many cases, the molecular orientation and arrangement are not homogeneously distributed in the whole polymer film. Since the mean free path of electrons is much smaller (few nm)[34] compared to photons, the comparison of spectra measured in TEY and FY modes allows us to distinguish differences of the molecular orientation on the surface of the polymer film and in the bulk of the 50 nm-thick films. In Figure 6, we compare relative intensities of angle-dependent XAS spectra measured simultaneously in TEY and FY modes for polymer **1a** on ITO and Au after post-deposition annealing. The corresponding spectra are shown in Figures S7 (FY) and S8 (TEY) (Supporting Information).

The data show that there are only very minor differences between the data points from TEY and FY spectra, revealing that the orientation of the polymer in the upper few nanometers is very similar to the bulk of the film with a thickness of about 50 nm.

This gives us the opportunity to compare the results of XAS in FY and TEY modes to a further, rather bulk sensitive method: PMIRRAS. PMIRRAS spectra of all four polymers in thin films of about 50 nm on Au are shown in Figure 7 before (blue curves) and after annealing (red curve) together with IR spectra of the polymers pressed in KBr pellets (black curves).

Although for molecules with a preferred orientation, particular vibration bands are suppressed due to the surface selection rules (e.g., refs 75−78), one can assume that the polymer powder in KBr exhibits a random orientation (i.e., average of all possible orientations). Thus, deviations from the black line in Figure 7 indicate a preferred orientation of the polymer in film. Clearly visible in Figure 7, very strong intensity variations can be observed for polymers **1a**, **2a**, and **2b** (see, e.g., bands at 800−850 cm^{-1}), whereas differences between the blue/red and black curve are minor for polymer **1b**. Thus, a preferred orientation for polymer **1b** is hardly visible. Already this qualitative comparison is in good agreement with the results of XAS measurements. For a detailed view, separated PMIRRAS spectra are shown in Figure S9, Supporting Information.

For a more quantitative approach, we calculated angles between the polymer backbone and substrate surface after Debe for PMIRRAS[21] and after Stöhr and Outka[73] for XAS measurements. We note that in both cases, these angles denote "average angles", that is, the angular distribution or the presence of partly disordered regions is neglected. For the calculation of angles from PMIRRAS, we used IR bands at about 1414 cm^{-1} (asymmetric stretching vibration, cyclopentadiene), 1377 cm^{-1} (symmetric stretching vibration, cyclopentadiene), and 825 cm^{-1} (out-of-plane vibration, C−H). Assignment of the bands to their corresponding vibrations follows DFT calculations (Figure S10 and Table S2, Supporting Information). The Euler angles Ψ (angle of *x* rotated around the surface normal) and Θ (angle between *z* and the surface normal) of the molecule's internal cartesian coordinates with respect to the surface normal were calculated according to $\sin^2\Psi = \frac{1}{1+r(zx)}$ and $\sin^2\Theta = \frac{1+r(zx)}{1+r(yx)+r(zx)}$,[21] where *x* is the intensity of the IR signal at 1414 cm^{-1}, *y* at 825 cm^{-1}, and *z* at 1377 cm^{-1}. These equations can be applied for moieties with C_{2v} symmetry (cyclopentadiene), as well as for D_2 and D_{2h} symmetry.[21,78] The angle between the polymer backbone and the sample surface is obtained from Euler angles by use of a rotation matrix (cf. ref 78).

For XAS, we determine the intensity ratio of two spectra measured at different angles of incoming light. Each intensity follows $I(\Phi) = P(\sin^2\alpha\,\sin^2\Phi + 2\cos^2\alpha\,\cos^2\Phi) + (1-P)\sin^2\alpha$, where Φ is the angle between the sample surface and incoming light, *P* the degree of polarization (we assume 0.95), and α is the tilt angle.

Angles between the polymer backbone and substrate surface from PMIRRAS and XAS are summarized in Table 4. In the case of XAS, both T and B1 intensities can be used to calculate the molecular orientation with respect to the substrate surface. In most cases, the results based on T and B1 intensities in Table 4 are in good agreement, and the small deviations might be due to the not pure in-plane or out-of-plane character of the transitions (cf. Figure 3) and restrictions of the peak fits with a single component. Most important, for all polymers, the calculated angles obtained from PMIRRAS are in excellent agreement with the XAS data. The agreement is the best for PMIRRAS and XAS obtained from thiophene subunit T. The all in all agreement shows that both complementary methods are well suited for determination of molecular orientation in thin films, at least, as long as the orientation is homogeneous in

Table 4. Angles between the Polymer Backbone and Substrate Surface from PMIRRAS and XAS[a]

polymer	1a	1b	2a	2b
	Room Temperature			
Au, PMIRRAS	20°	34°	22°	21°
ITO, XAS T	24°	33°	21°	23°
ITO, XAS B_1	22°	34°	17°	21°
	Annealed (130 °C)			
Au, PMIRRAS	14°	34°	23°	23°
ITO (Au), XAS T	17° (18°)	29° (36°)	19°	22°
ITO (Au), XAS B_1	12° (15°)	22° (34°)	10°	17°

[a]Noticeably, in agreement with XAS results, average tilt angles for polymer **1b** are significantly larger, which may indicate a higher degree of disorder. Both methods XAS and PMIRRAS deliver very similar, complementary results.

https://doi.org/10.1021/acsaem.2c02919
ACS Appl. Energy Mater. 2022, 5, 15290−15301

the whole film as for the studied polymers. We note that a preferred molecular orientation implies a high degree of ordering and a high ability of self-organization. However, vice-versa, if we find no preferred molecular orientation, a high ordering in the film cannot be ruled out completely.

4. CONCLUSIONS

We have shown that neither the introduction of oxygen nor the alternating position of the side chains has a notable influence on the position of charge transfer levels at the studied interfaces, in spite of the optical gap and the ionization potential changes. Highest ionization potentials and optical gap are observed for polymers with alkyl side chains.

In contrast, the preferred molecular orientation, indicating a high degree of ordering, depends strongly on the position and kind (alkyl or alkoxy) of the side chain at the thienylene spacers. The comparison of polymers **1a** and **1b** shows that the exact position of the alkyl side chain might be crucial for the molecular orientation. Post-deposition annealing can increase the tendency significantly of a preferred "face-on" orientation in all cases.

The homogeneous molecular orientation within the 50 nm-thick films enables the comparison of different methods for the determination of the molecular orientation with different surface sensitivities: XAS in FY and TEY modes and PMIRRAS. All methods deliver comparable and consistent information about orientation of polymers in thin films.

■ ASSOCIATED CONTENT

Supporting Information

The Supporting Information is available free of charge at https://pubs.acs.org/doi/10.1021/acsaem.2c02919.

> UPS HeI spectra, UV/vis spectra of polymers in thin films and in solution, energy level alignment diagrams, XAS of the ITO substrate measured in FY and TEY modes, EDX of the ITO substrate, S K edge XAS spectra: zoom into the low photon energy region, additional peak fits of S K edge XAS spectra, separated PMIRRAS spectra, B3LYP/6-31G* calculated IR spectra and assignment, stoichiometric composition in polymer thin films as obtained from XPS, vibrational frequencies and assigned vibrations, and synthesis of the polymers (general procedure) (PDF)

■ AUTHOR INFORMATION

Corresponding Author

Heiko Peisert − *Institut für Physikalische und Theoretische Chemie, Eberhard Karls Universität Tübingen, 72076 Tübingen, Germany;* orcid.org/0000-0002-9742-5800; Email: heiko.peisert@uni-tuebingen.de

Authors

Sven Bölke − *Institut für Physikalische und Theoretische Chemie, Eberhard Karls Universität Tübingen, 72076 Tübingen, Germany*

David Batchelor − *Karlsruher Institut für Technologie, Institute for Photon Science and Synchrotron Radiation (IPS), D-76344 Eggenstein-Leopoldshafen, Germany*

Andreas Früh − *Institut für Physikalische und Theoretische Chemie, Eberhard Karls Universität Tübingen, 72076 Tübingen, Germany*

Benedikt Lassalle-Kaiser − *Synchrotron SOLEIL, 91190 Saint-Aubin, France;* orcid.org/0000-0003-2141-2496

Tina Keller − *Makromolekulare Chemie (buwMakro) und Wuppertal Center for Smart Materials and Systems (CM@S), Bergische Universität Wuppertal, 42119 Wuppertal, Germany*

Florian Trilling − *Makromolekulare Chemie (buwMakro) und Wuppertal Center for Smart Materials and Systems (CM@S), Bergische Universität Wuppertal, 42119 Wuppertal, Germany;* orcid.org/0000-0001-6096-7895

Michael Forster − *Makromolekulare Chemie (buwMakro) und Wuppertal Center for Smart Materials and Systems (CM@S), Bergische Universität Wuppertal, 42119 Wuppertal, Germany*

Ullrich Scherf − *Makromolekulare Chemie (buwMakro) und Wuppertal Center for Smart Materials and Systems (CM@S), Bergische Universität Wuppertal, 42119 Wuppertal, Germany;* orcid.org/0000-0001-8368-4919

Thomas Chassé − *Institut für Physikalische und Theoretische Chemie, Eberhard Karls Universität Tübingen, 72076 Tübingen, Germany;* orcid.org/0000-0001-6442-8944

Complete contact information is available at: https://pubs.acs.org/10.1021/acsaem.2c02919

Notes

The authors declare no competing financial interest.

■ ACKNOWLEDGMENTS

The authors acknowledge support by the state of Baden-Württemberg through bwHPC and the German Research Foundation (DFG) through grant numbers PE 546/10-3, CH132/24-3, SCHE410/24-3, and INST 40/575-1 FUGG (JUSTUS 2 cluster). We are grateful to the synchrotron SOLEIL (Paris, France) for the provision of beamtime and the assistance from SOLEIL beamline staff. We thank Katharina Greulich (University of Tübingen) for valuable discussions and Lennart Rieger (University of Tübingen) for the support of PM-IRRAS measurements.

■ REFERENCES

(1) Li, Y.; Xu, G.; Cui, C. H.; Li, Y. F. Flexible and Semitransparent Organic Solar Cells. *Adv. Energy Mater.* **2018**, *8*, 1701791.

(2) Khandelwal, K.; Biswas, S.; Mishra, A.; Sharma, G. D. Semitransparent Organic Solar Cells: From Molecular Design to Structure-Performance Relationships. *J. Mater. Chem. C* **2021**, *10*, 13−43.

(3) Bonnassieux, Y.; Brabec, C. J.; Cao, Y.; Carmichael, T. B.; Chabinyc, M. L.; Cheng, K. T.; Cho, G.; Chung, A.; Cobb, C. L.; Distler, A.; Egelhaaf, H. J.; Grau, G.; Guo, X. J.; Haghiashtiani, G.; Huang, T. C.; Hussain, M. M.; Iniguez, B.; Lee, T. M.; Li, L.; Ma, Y. G.; Ma, D. G.; McAlpine, M. C.; Ng, T. N.; Osterbacka, R.; Patel, S. N.; Peng, J. B.; Peng, H. S.; Rivnay, J.; Shao, L. L.; Steingart, D.; Street, R. A.; Subramanian, V.; Torsi, L.; Wu, Y. Y. The 2021 Flexible and Printed Electronics Roadmap. *Flexible Printed Electron.* **2022**, *6*, 023001.

(4) Brabec, C. J.; Gowrisanker, S.; Halls, J. J. M.; Laird, D.; Jia, S. J.; Williams, S. P. Polymer-Fullerene Bulk-Heterojunction Solar Cells. *Adv. Mater.* **2010**, *22*, 3839−3856.

(5) Hou, J. H.; Inganäs, O.; Friend, R. H.; Gao, F. Organic Solar Cells Based on Non-Fullerene Acceptors. *Nat. Mater.* **2018**, *17*, 119−128.

(6) Cui, Y.; Yao, H.; Zhang, J.; Zhang, T.; Wang, Y.; Hong, L.; Xian, K.; Xu, B.; Zhang, S.; Peng, J.; Wei, Z.; Gao, F.; Hou, J. Over 16% Efficiency Organic Photovoltaic Cells Enabled by a Chlorinated

Acceptor with Increased Open-Circuit Voltages. *Nat. Commun.* **2019**, *10*, 2515.
(7) Liu, C.; Xiao, C. Y.; Xie, C. C.; Li, W. W. Flexible Organic Solar Cells: Materials, Large-Area Fabrication Techniques and Potential Applications. *Nano Energy* **2021**, *89*, 106399.
(8) Armin, A.; Li, W.; Sandberg, O. J.; Xiao, Z.; Ding, L. M.; Nelson, J.; Neher, D.; Vandewal, K.; Shoaee, S.; Wang, T.; Ade, H.; Heumuller, T.; Brabec, C.; Meredith, P. A History and Perspective of Non-Fullerene Electron Acceptors for Organic Solar Cells. *Adv. Energy Mater.* **2021**, *11*, 2003570.
(9) Fan, B. B.; Du, X. Y.; Liu, F.; Zhong, W. K.; Ying, L.; Xie, R. H.; Tang, X. F.; An, K.; Xin, J. M.; Li, N.; Ma, W.; Brabec, C. J.; Huang, F.; Cao, Y. Fine-Tuning of the Chemical Structure of Photoactive Materials for Highly Efficient Organic Photovoltaics. *Nat. Energy* **2018**, *3*, 1051−1058.
(10) Aygül, U.; Peisert, H.; Batchelor, D.; Dettinger, U.; Ivanovic, M.; Tournebize, A.; Mangold, S.; Förster, M.; Dumsch, I.; Kowalski, S.; Allard, S.; Scherf, U.; Chassé, T. Molecular Orientation in Polymer/Fullerene Blend Films and the Influence of Annealing. *Sol. Energy Mater. Sol. Cells* **2014**, *128*, 119−125.
(11) Kanai, K.; Miyazaki, T.; Suzuki, H.; Inaba, M.; Ouchi, Y.; Seki, K. Effect of Annealing on the Electronic Structure of Poly(3-Hexylthiophene) Thin Film. *Phys. Chem. Chem. Phys.* **2010**, *12*, 273−282.
(12) Chang, J.-F.; Sun, B.; Breiby, D. W.; Nielsen, M. M.; Sölling, T. I.; Giles, M.; McCulloch, I.; Sirringhaus, H. Enhanced Mobility of Poly(3-Hexylthiophene) Transistors by Spin-Coating from High-Boiling-Point Solvents. *Chem. Mater.* **2004**, *16*, 4772−4776.
(13) Batchelor, D. R.; Aygül, U.; Dettinger, U.; Ivanovic, M.; Tournebize, A.; Mangold, S.; Forster, M.; Scherf, U.; Peisert, H.; Chassé, T. Insight into the Orientation of Lbg Polymer Films by XANES Experiment and Calculation. *Eur. Polym. J.* **2016**, *81*, 686−693.
(14) Ivanović, M.; Aygül, U.; Dettinger, U.; Tournebize, A.; Polek, M.; Batchelor, D.; Mangold, S.; Forster, M.; Scherf, U.; Peisert, H.; Chassé, T. Electronic Structure and Self-Organization Properties of Low Band Gap Polymers: The Effect of the Introduction of Additional Thiophene Moieties. *Sol. Energy Mater. Sol. Cells* **2016**, *157*, 286−294.
(15) Borges, B.; Veiga, A. G.; Gioti, M.; Laskarakis, A.; Tzounis, L.; Logothetidis, S.; Rocco, M. L. M. Surface, Interface and Electronic Properties of F8:F8bt Polymeric Thin Films Used for Organic Light-Emitting Diode Applications. *Polym. Int.* **2018**, *67*, 691−699.
(16) Borges, B.; Veiga, A. G.; Tzounis, L.; Laskarakis, A.; Logothetidis, S.; Rocco, M. L. M. Molecular Orientation and Ultrafast Charge Transfer Dynamics Studies on the P3ht:Pcbm Blend. *J. Phys. Chem. C* **2016**, *120*, 25078−25082.
(17) Aygül, U.; Batchelor, D.; Dettinger, U.; Yilmaz, S.; Allard, S.; Scherf, U.; Peisert, H.; Chassé, T. Molecular Orientation in Polymer Films for Organic Solar Cells Studied by NEXAFS. *J. Phys. Chem. C* **2012**, *116*, 4870−4874.
(18) Niwa, H.; Horiba, K.; Harada, Y.; Oshima, M.; Ikeda, T.; Terakura, K.; Ozaki, J.-i.; Miyata, S. X-Ray Absorption Analysis of Nitrogen Contribution to Oxygen Reduction Reaction in Carbon Alloy Cathode Catalysts for Polymer Electrolyte Fuel Cells. *J. Power Sources* **2009**, *187*, 93−97.
(19) Meng, N.; Ren, J.; Liu, Y.; Huang, Y.; Petit, T.; Zhang, B. Engineering Oxygen-Containing and Amino Groups into Two-Dimensional Atomically-Thin Porous Polymeric Carbon Nitrogen for Enhanced Photocatalytic Hydrogen Production. *Energy Environ. Sci.* **2018**, *11*, 566−571.
(20) Erbil, A.; Cargill III, G. S., Iii; Frahm, R.; Boehme, R. F. Total-Electron-Yield Current Measurements for near-Surface Extended X-Ray-Absorption Fine Structure. *Phys. Rev. B: Condens. Matter Mater. Phys.* **1988**, *37*, 2450−2464.
(21) Debe, M. K. Extracting Physical Structure Information from Thin Organic Films with Reflection Absorption Infrared Spectroscopy. *J. Appl. Phys.* **1984**, *55*, 3354−3366.
(22) Gliboff, M.; Sang, L.; Knesting, K. M.; Schalnat, M. C.; Mudalige, A.; Ratcliff, E. L.; Li, H.; Sigdel, A. K.; Giordano, A. J.; Berry, J. J.; Nordlund, D.; Seidler, G. T.; Brédas, J.-L.; Marder, S. R.; Pemberton, J. E.; Ginger, D. S. Orientation of Phenylphosphonic Acid Self-Assembled Monolayers on a Transparent Conductive Oxide: A Combined NEXAFS, Pm-Irras, and Dft Study. *Langmuir* **2013**, *29*, 2166−2174.
(23) An, L. L.; Duan, Y. X.; Yuan, Y.; Zhou, L. J.; Zhang, J. M. Effect of Thermal Annealing on the Microstructure of P3ht Thin Film Investigated by Rair Spectroscopy. *Vib. Spectrosc.* **2013**, *68*, 40−44.
(24) Sang, L.; Mudalige, A.; Sigdel, A. K.; Giordano, A. J.; Marder, S. R.; Berry, J. J.; Pemberton, J. E. Pm-Irras Determination of Molecular Orientation of Phosphonic Acid Self-Assembled Monolayers on Indium Zinc Oxide. *Langmuir* **2015**, *31*, 5603−5613.
(25) Shioya, N.; Shimoaka, T.; Hasegawa, T. Analysis of Molecular Orientation and Conformation of Poly(3-Hexylthiophene) Thin Films on Silicon by Infrared P-Polarized Multiple-Angle Incidence Resolution Spectrometry. *Chem. Lett.* **2014**, *43*, 1198−1200.
(26) Osaka, I.; Saito, M.; Koganezawa, T.; Takimiya, K. Thiophene−Thiazolothiazole Copolymers: Significant Impact of Side Chain Composition on Backbone Orientation and Solar Cell Performances. *Adv. Mater.* **2014**, *26*, 331−338.
(27) Saito, M.; Ogawa, S.; Osaka, I. Contrasting Effect of Side-Chain Placement on Photovoltaic Performance of Binary and Ternary Blend Organic Solar Cells in Benzodithiophene-Thiazolothiazole Polymers. *Chemsuschem* **2021**, *14*, 5032−5041.
(28) Stille, J. K. The Palladium-Catalyzed Cross-Coupling Reactions of Organotin Reagents with Organic Electrophiles. *Angew. Chem., Int. Ed. Engl.* **1986**, *25*, 508−524.
(29) Cordovilla, C.; Bartolomé, C.; Martínez-Ilarduya, J. M.; Espinet, P. The Stille Reaction, 38 Years Later. *ACS Catal.* **2015**, *5*, 3040−3053.
(30) Zhang, M.; Tsao, H. N.; Pisula, W.; Yang, C. D.; Mishra, A. K.; Müllen, K. Field-Effect Transistors Based on a Benzothiadiazole-Cyclopentadithiophene Copolymer. *J. Am. Chem. Soc.* **2007**, *129*, 3472.
(31) Mühlbacher, D.; Scharber, M.; Morana, M.; Zhu, Z. G.; Waller, D.; Gaudiana, R.; Brabec, C. High Photovoltaic Performance of a Low-Bandgap Polymer (Vol 18, Pg 2884, 2006). *Adv. Mater.* **2006**, *18*, 2931.
(32) Silva, H. S.; Tournebize, A.; Bégué, D.; Peisert, H.; Chassé, T.; Gardette, J. L.; Therias, S.; Rivaton, A.; Hiorns, R. C. A Universal Route to Improving Conjugated Macromolecule Photostability. *RSC Adv.* **2014**, *4*, 54919−54923.
(33) Yeh, J. J.; Lindau, I. Atomic Subshell Photoionization Cross Sections and Asymmetry Parameters: $1 \leqslant Z \leqslant 103$. *At. Data Nucl. Data Tables* **1985**, *32*, 1−155.
(34) Seah, M. P.; Dench, W. A. Quantitative Electron Spectroscopy of Surfaces: A Standard Data Base for Electron Inelastic Mean Free Paths in Solids. *Surf. Interface Anal.* **1979**, *1*, 2−11.
(35) Vantelon, D.; Trcera, N.; Roy, D.; Moreno, T.; Mailly, D.; Guilet, S.; Metchalkov, E.; Delmotte, F.; Lassalle, B.; Lagarde, P.; Flank, A.-M. The Lucia Beamline at Soleil. *J. Synchrotron Radiat.* **2016**, *23*, 635−640.
(36) Hesse, R.; Weiß, M.; Szargan, R.; Streubel, P.; Denecke, R. Comparative Study of the Modelling of the Spectral Background of Photoelectron Spectra with the Shirley and Improved Tougaard Methods. *J. Electron Spectrosc. Relat. Phenom.* **2013**, *186*, 44−53.
(37) Neese, F. The ORCA program system. *Wiley Interdiscip. Rev.: Comput. Mol. Sci.* **2012**, *2*, 73−78.
(38) *Gaussian 16* Rev. C.01: Wallingford, CT, 2016.
(39) Halls, M. D.; Velkovski, J.; Schlegel, H. B. Harmonic Frequency Scaling Factors for Hartree-Fock, S-Vwn, B-Lyp, B3-Lyp, B3-Pw91 and Mp2 with the Sadlej Pvtz Electric Property Basis Set. *Theor. Chem. Acc.* **2001**, *105*, 413−421.
(40) Zapata Trujillo, J. C.; McKemmish, L. K. Meta-Analysis of Uniform Scaling Factors for Harmonic Frequency Calculations. *Wiley Interdiscip. Rev.: Comput. Mol. Sci.* **2022**, *12*, No. e1584.

(41) Irikura, K. K.; Johnson, R. D.; Kacker, R. N. Uncertainties in Scaling Factors for Ab Initio Vibrational Frequencies. *J. Phys. Chem. A* **2005**, *109*, 8430−8437.
(42) Zade, S. S.; Bendikov, M. Cyclic Oligothiophenes: Novel Organic Materials and Models for Polythiophene. A Theoretical Study. *J. Org. Chem.* **2006**, *71*, 2972−2981.
(43) Zade, S. S.; Zamoshchik, N.; Bendikov, M. Oligo- and Polyselenophenes: A Theoretical Study. *Chem. - Eur. J.* **2009**, *15*, 8613−8624.
(44) Beamson, G.; Briggs, D.*High Resolution XPS of Organic Polymers: The Scienta Esca300 Database*; Wiley: New York, 1992.
(45) Aygül, U.; Peisert, H.; Frisch, J.; Vollmer, A.; Koch, N.; Chassé, T. Electronic Properties of Interfaces between Pcpdtbt and Prototypical Electrodes Studied by Photoemission Spectroscopy. *ChemPhysChem* **2011**, *12*, 2345−2351.
(46) Peisert, H.; Knupfer, M.; Schwieger, T.; Fuentes, G. G.; Olligs, D.; Fink, J.; Schmidt, T. Fluorination of Copper Phthalocyanines: Electronic Structure and Interface Properties. *J. Appl. Phys.* **2003**, *93*, 9683−9692.
(47) Tauc, J. Optical Properties and Electronic Structure of Amorphous Ge and Si. *Mater. Res. Bull.* **1968**, *3*, 37−46.
(48) Duhm, S.; Heimel, G.; Salzmann, I.; Glowatzki, H.; Johnson, R. L.; Vollmer, A.; Rabe, J. P.; Koch, N. Orientation-Dependent Ionization Energies and Interface Dipoles in Ordered Molecular Assemblies. *Nat. Mater.* **2008**, *7*, 326−332.
(49) Ivanco, J.; Krenn, J. R.; Ramsey, M. G.; Netzer, F. P.; Haber, T.; Resel, R.; Haase, A.; Stadlober, B.; Jakopic, G. Sexithiophene Films on Clean and Oxidized Si(111) Surfaces: Growth and Electronic Structure. *J. Appl. Phys.* **2004**, *96*, 2716−2724.
(50) Braun, S.; Salaneck, W. R.; Fahlman, M. Energy-Level Alignment at Organic/Metal and Organic/Organic Interfaces. *Adv. Mater.* **2009**, *21*, 1450−1472.
(51) Bokdam, M.; Çakır, D.; Brocks, G. Fermi Level Pinning by Integer Charge Transfer at Electrode-Organic Semiconductor Interfaces. *Appl. Phys. Lett.* **2011**, *98*, 113303.
(52) Bao, Q.; Sandberg, O.; Dagnelund, D.; Sandén, S.; Braun, S.; Aarnio, H.; Liu, X.; Chen, W. M.; Österbacka, R.; Fahlman, M. Trap-Assisted Recombination Via Integer Charge Transfer States in Organic Bulk Heterojunction Photovoltaics. *Adv. Funct. Mater.* **2014**, *24*, 6309−6316.
(53) Fahlman, M.; Sehati, P.; Osikowicz, W.; Braun, S.; de Jong, M. P.; Brocks, G. Photoelectron Spectroscopy and Modeling of Interface Properties Related to Organic Photovoltaic Cells. *J. Electron Spectrosc. Relat. Phenom.* **2013**, *190*, 33−41.
(54) Fahlman, M.; Crispin, A.; Crispin, X.; Henze, S. K. M.; de Jong, M. P.; Osikowicz, W.; Tengstedt, C.; Salaneck, W. R. Electronic Structure of Hybrid Interfaces for Polymer-Based Electronics. *J. Phys.: Condens. Matter* **2007**, *19*, 20.
(55) Hofmann, O. T.; Rinke, P.; Scheffler, M.; Heimel, G. Integer Versus Fractional Charge Transfer at Metal(/Insulator)/Organic Interfaces: Cu(/Nacl)/Tcne. *ACS Nano* **2015**, *9*, 5391−5404.
(56) Wang, Q.; Yang, J.; Gerlach, A.; Schreiber, F.; Duhm, S. Advanced Characterization of Organic-Metal and Organic-Organic Interfaces: From Photoelectron Spectroscopy Data to Energy-Level Diagrams. *J. Phys.: Mater.* **2022**, *5*, 044010.
(57) Endo, O.; Matsui, F.; Kera, S.; Chun, W. J.; Nakamura, M.; Amemiya, K.; Ozaki, H. Observation of Hole States at Perylene/Au(110) and Au(111) Interfaces. *J. Phys. Chem. C* **2022**, *126*, 15971−15979.
(58) Winkler, S.; Amsalem, P.; Frisch, J.; Oehzelt, M.; Heimel, G.; Koch, N. Probing the Energy Levels in Hole-Doped Molecular Semiconductors. *Mater. Horiz.* **2015**, *2*, 427−433.
(59) Hollerer, M.; Lüftner, D.; Hurdax, P.; Ules, T.; Soubatch, S.; Tautz, F. S.; Koller, G.; Puschnig, P.; Sterrer, M.; Ramsey, M. G. Charge Transfer and Orbital Level Alignment at Inorganic/Organic Interfaces: The Role of Dielectric Interlayers. *ACS Nano* **2017**, *11*, 6252−6260.
(60) Chen, Y.; Liu, X.; Braun, S.; Wang, Y.; Fahlman, M. Image-Force Effects on Energy Level Alignment at Electron Transport Material/Cathode Interfaces. *J. Mater. Chem. C* **2020**, *8*, 173−179.
(61) Hitchcock, A. P.; DeWitte, R. S.; Van Esbroeck, J. M.; Aebi, P.; Frenc, C. L.; Oakley, R. T.; Westwood, N. P. C. A Valence- and Inner-Shell Electronic and Photoelectron Spectroscopic Study of the Frontier Orbitals of 2,1,3-Benzothiadiazole, C6h4sn2, 1,3,2,4-Benzodithiadiazine, C6h4s2n2, and 1,3,5,2,4-Benzotrithiadiazepine, C6h4s3n2. *J. Electron Spectrosc. Relat. Phenom.* **1991**, *57*, 165−187.
(62) Hitchcock, A. P.; Horsley, J. A.; Stöhr, J. Inner Shell Excitation of Thiophene and Thiolane: Gas, Solid, and Monolayer States. *J. Chem. Phys.* **1986**, *85*, 4835−4848.
(63) Garcia-Basabe, Y.; Marchiori, C. F. N.; Borges, B. G. A. L.; Yamamoto, N. A. D.; Macedo, A. G.; Koehler, M.; Roman, L. S.; Rocco, M. L. M. Electronic Structure, Molecular Orientation, Charge Transfer Dynamics and Solar Cells Performance in Donor/Acceptor Copolymers and Fullerene: Experimental and Theoretical Approaches. *J. Appl. Phys.* **2014**, *115*, 134901.
(64) Araújo, G.; Arantes, C.; Roman, L. S.; Zarbin, A. J. G.; Rocco, M. L. M. Photoabsorption and Desorption Studies on Poly-3-Hexylthiophene/Multi-Walled Carbon Nanotube Composite Films. *Surf. Sci.* **2009**, *603*, 647−652.
(65) Xue, B.; Vaughan, B.; Poh, C.-H.; Burke, K. B.; Thomsen, L.; Stapleton, A.; Zhou, X.; Bryant, G. W.; Belcher, W.; Dastoor, P. C. Vertical Stratification and Interfacial Structure in P3ht:Pcbm Organic Solar Cells. *J. Phys. Chem. C* **2010**, *114*, 15797−15805.
(66) Germack, D. S.; Chan, C. K.; Kline, R. J.; Fischer, D. A.; Gundlach, D. J.; Toney, M. F.; Richter, L. J.; DeLongchamp, D. M. Interfacial Segregation in Polymer/Fullerene Blend Films for Photovoltaic Devices. *Macromolecules* **2010**, *43*, 3828−3836.
(67) Ma, W.; Yang, C.; Gong, X.; Lee, K.; Heeger, A. J. Thermally Stable, Efficient Polymer Solar Cells with Nanoscale Control of the Interpenetrating Network Morphology. *Adv. Funct. Mater.* **2005**, *15*, 1617−1622.
(68) Motaung, D.; Malgas, G.; Arendse, C.; Mavundla, S.; Oliphant, C.; Knoesen, D. The Influence of Thermal Annealing on the Morphology and Structural Properties of a Conjugated Polymer in Blends with an Organic Acceptor Material. *J. Mater. Sci.* **2009**, *44*, 3192−3197.
(69) Wu, W.-R.; Jeng, U. S.; Su, C.-J.; Wei, K.-H.; Su, M.-S.; Chiu, M.-Y.; Chen, C.-Y.; Su, W.-B.; Su, C.-H.; Su, A.-C. Competition between Fullerene Aggregation and Poly(3-Hexylthiophene) Crystallization Upon Annealing of Bulk Heterojunction Solar Cells. *ACS Nano* **2011**, *5*, 6233−6243.
(70) Zhu, W. G.; Spencer, A. P.; Mukherjee, S.; Alzola, J. M.; Sangwan, V. K.; Amsterdam, S. H.; Swick, S. M.; Jones, L. O.; Heiber, M. C.; Herzing, A. A.; Li, G. P.; Stern, C. L.; DeLongchamp, D. M.; Kohlstedt, K. L.; Hersam, M. C.; Schatz, G. C.; Wasielewski, M. R.; Chen, L. X.; Facchetti, A.; Marks, T. J. Crystallography, Morphology, Electronic Structure, and Transport in Non-Fullerene/Non-Indacenodithienothiophene Polymer:Y6 Solar Cells. *J. Am. Chem. Soc.* **2020**, *142*, 14532−14547.
(71) Lee, J. S.; Prabu, A. A.; Kim, K. J. Annealing Effect Upon Chain Orientation, Crystalline Morphology, and Polarizability of Ultra-Thin P(Vdf-Trfe) Film for Nonvolatile Polymer Memory Device. *Polymer* **2010**, *51*, 6319−6333.
(72) Bolognesi, A.; Botta, C.; Mercogliano, C.; Marinelli, M.; Porzio, W.; Angiolini, L.; Salatelli, E. Oriented Thin Films from Soluble Polythiophenes. *Polym. Adv. Technol.* **2003**, *14*, 537−543.
(73) Stöhr, J.; Outka, D. A. Determination of Molecular Orientations on Surfaces from the Angular Dependence of near-Edge X-Ray-Absorption Fine-Structure Spectra. *Phys. Rev. B: Condens. Matter Mater. Phys.* **1987**, *36*, 7891−7905.
(74) Peisert, H.; Biswas, I.; Knupfer, M.; Chassé, T. Orientation and Electronic Properties of Phthalocyanines on Polycrystalline Substrates. *Phys. Status Solidi B* **2009**, *246*, 1529−1545.
(75) Pearce, H. A.; Sheppard, N. Possible Importance of a Metal-Surface Selection Rule in Interpretation of Infrared-Spectra of Molecules Adsorbed on Particulate Metals - Infrared-Spectra from

https://doi.org/10.1021/acsaem.2c02919
ACS Appl. Energy Mater. 2022, 5, 15290−15301

Ethylene Chemisorbed on Silica-Supported Metal-Catalysts. *Surf. Sci.* **1976**, *59*, 205−217.
(76) Greenler, R. G. Infrared Study of Adsorbed Molecules on Metal Surfaces by Reflection Techniques. *J. Chem. Phys.* **1966**, *44*, 310−315.
(77) Umemura, J.Reflection−Absorption Spectroscopy of Thin Films on Metallic Substrates. *Handbook of Vibrational Spectroscopy*; John Wiley & Sons, 2001.
(78) Früh, A.; Rutkowski, S.; Akimchenko, I. O.; Tverdokhlebov, S. I.; Frueh, J. Orientation Analysis of Polymer Thin Films on Metal Surfaces Via Ir Absorbance of the Relative Transition Dipole Moments. *Appl. Surf. Sci.* **2022**, *594*, 153476.

https://doi.org/10.1021/acsaem.2c02919
ACS Appl. Energy Mater. 2022, 5, 15290−15301